The 400d X-ray Survey: The Weak Lensing Follow-Up Programme

Holger Israel[1,4], Thomas Reiprich[1], Thomas Erben[1], Daniel Hudson[1], Peter Schneider[1], Alexey Vikhlinin[2], Craig Sarazin[3], & Kenneth Rines[2]

[1] Argelander-Institut für Astronomie, Auf dem Hügel 71, 53121 Bonn, Germany
[2] Harvard-Smithsonian Center for Astrophysics, 60 Garden Street, Cambridge, MA 02138, USA
[3] Departement of Astronomy, University of Virginia, 530 McCormick Road, Charlottesville, VA 22904, USA
[4] e-mail: hisrael@astro.uni-bonn.de

Argelander-Institut für Astronomie

Abstract: Evolution in the mass function of galaxy clusters sensitively traces cosmological structure formation. The number density of massive clusters as a function of z can be used to constrain cosmological parameters. We aim at deriving a robust mass function by a detailed comparison of cluster masses deduced from observations of their X-ray and weak lensing signals. Based on the recent *400d* survey of serendipitous ROSAT detections, we therefore use a complete X-ray flux- and luminosity-limited subsample of clusters at $z \geq 0.35$ for which we conduct a weak lensing follow-up survey. We report first results of our weak lensing analysis based on observations obtained with the MMT Megacam camera.

Weak Lensing Observations for a New X-Ray Selected Distant Cluster Sample

Sample Definition: Based on the *400d* survey of galaxy clusters serendipitously detected in the complete set of suitable ROSAT PSPC pointings (Burenin et al. 2007), we define a subsample for cosmological studies. In this high-redshift sample, all *400d* clusters at redshift $z \geq 0.35$ and X-ray luminosity exceeding $L_{\mathrm{X,min}} \geq 4.8 10^{43} (1+z)^{1.8} \mathrm{erg/s}$ in standard ΛCDM cosmology are included (see Vikhlinin et al. 2008). The resulting sample consists of 40 galaxy clusters which can be nearly equally distributed in three redshift bins $0.35 \leq z < 0.45$, $0.45 \leq z < 0.55$, and $0.55 \leq z < 0.90$ for which we seek to derive the mass function. While the evolution in their redshift regime is strong, these clusters inhabit a mass range typical for the *local* Universe, and are therefore ideal for a comparison with the *HIFLUGCS* sample at $\bar{z} = 0.05$.

MMT Observations: have been obtained with the $24' \times 24'$ MEGACAM wide-field imager in Oct. 2004, June 2005, Oct./Nov. 2005, and Jan. 2008. MEGACAM, a mosaic of 36 CCDs, 2048×4608 pixels each, is located at the 6.5 m MMT telescope at Whipple Observatory, Mt. Hopkins, Arizona. **Observation Strategy:** Lensing analysis is based on deep imaging in the r' band aiming at the highest possible number of faint background galaxies suitable for shape measurements. We employ a *dither pattern* to obtain homogeneous data quality throughout the field of view despite gaps between camera chips. Additional g' and i' imaging will be included to identify cluster members and select catalogues by colours.

Reduction of MMT/MEGACAM data

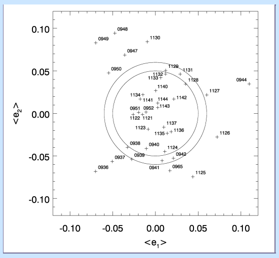

Figure 1: Anisotropy of the PSF in Several Frames

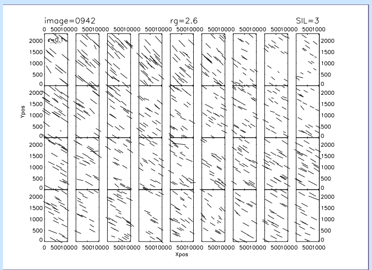

Figure 2: Spatial Variation of PSF Anisotropy

Reduction Pipeline and Weak Lensing Analysis

- Data reduction is carried out using the THELI pipeline (cf. Erben et al. 2005) designed for processing wide-field data from mosaic cameras. For improved robustness of the astrometric solution, we implemented SWARP into the pipeline.
- Weak lensing information is extracted from coadded images using an implementation of the KSB+ algorithm based on the one presented by T. Schrabback in Heymans et al. (2006).

Figure 1: Mean stellar anisotropies $\langle e_{1,2} \rangle$ found in the r'-band frames of CL0030+2618 fulfilling the seeing condition $s < 1.0''$. All images with $\langle |e| \rangle < 0.05$ are included in the final coaddition (inner circle), while those exceeding $\langle |e| \rangle < 0.06$ (outer circle) are always rejected. The decision for intermediary objects (see below) is based on visual inspection.

Figure 2: Stellar anisotropies as a function of position on MEGACAMs detecting surface. Shown as an example is one (#0942) of the r'-images of CL0030+2618 classified within the critical $0.05 < \langle |e| \rangle < 0.06$ range shown in Figure 1. Note that there are **no jumps at chip borders** in any MMT images we analysed up to now. Still, this image suffers from a bad PSF due to imperfect tracking and is therefore rejected.

Figure 3: PSF anisotropy correction. Plotted are the ellipticities of sources identified as stars in the coadded image of the CL0030+2618 field (left panels), a polynomial model $e^{\mathrm{an}}1,2(x,y)$ to the PSF anisotropy (middle panels). and the residuals after subtraction of the model (right panels). The orientations of the anisotropy-corrected stellar ellipticities are effectively randomised.

Figure 4: Colour-colour-diagrammes of objects classified as galaxies in the field of CL0030+2618. The g'-r' vs. r'-i' colours of galaxies in three magnitude bins are plotted. Blue: Sources with $r' < 22.5$ populate a well-defined region in the diagramme. They are very likely to be foreground or cluster sources. Black: Sources with $r' > 23.5$ tend to have bluer g'-r' colours and can be assumed to be in the background. Green: The intermediate bin of $22.5 < r' < 23.5$ marks the transition between both regimes. Objects in the orange polygon follow the colours of the foreground sources and are interpreted to either reside in the cluster or foreground. Sources outside the polygon, we identify as background galaxies and include them into the lensing catalogue.

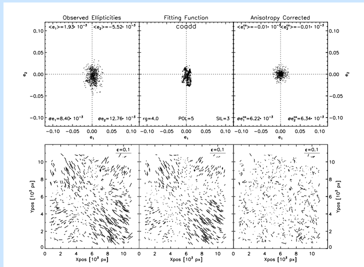

Figure 3: Correction of PSF Anisotropy

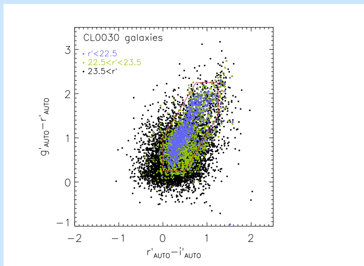

Figure 4: Colour-Colour Selection of Background Objects

First Results: the Eight *400d* Clusters Observed with MMT/MEGACAM

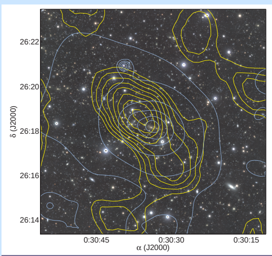

Figure 5: Detections of CL0030+2618. Shown is a composite of the central parts of our coadded g', r', and i' images. Overlaid in blue are CHANDRA X-ray contours , while yellow contours give the significance of aperture mass detection, spaced in intervals in S/N of 0.5, starting at $S/N = 0.5$.

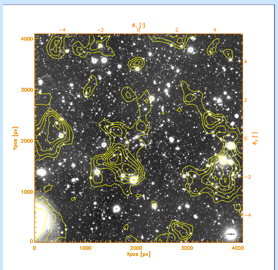

Figure 6: CL1701+6414, central $11' \times 11'$ of the coadded r'-image overlaid with M_{ap} significance contours as in Figure 5. The Schirmer et al. (2004) filter is used at $\theta_{\mathrm{out}} = 4.8'$.

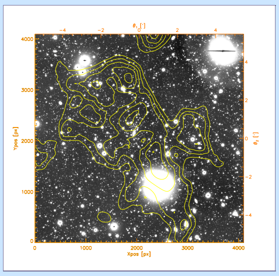

Figure 7: CL1641+4001, central $11' \times 11'$ of the coadded r'-image overlaid with M_{ap} significance contours as in Fig. 5. The Schirmer et al. (2004) filter is used at $\theta_{\mathrm{out}} = 8'$.

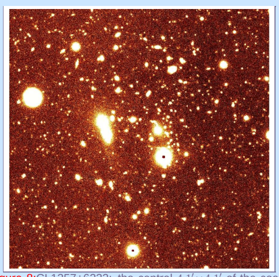

Figure 8: CL1357+6232: the central $4.1' \times 4.1'$ of the coadded r'-image.

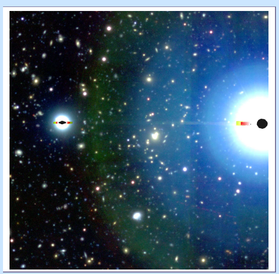

Figure 9: CL0159+0030: central $4.1' \times 4.1'$ of $g'r'i'$-composite.

Figure 10: CL0230+1836: central $4.1' \times 4.1'$ of $g'r'i'$-composite.

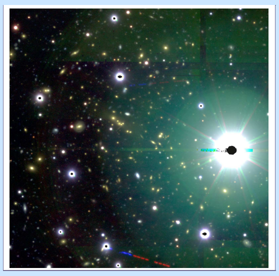

Figure 11: CL0809+2811: $g'r'i'$-composite, central $4.1' \times 4.1'$.

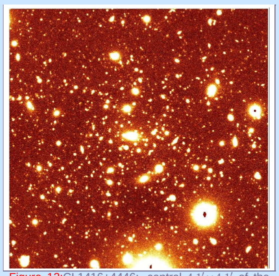

Figure 12: CL1416+4446: central $4.1' \times 4.1'$ of the coadded r'-image.

References

Burenin, R. A., Vikhlinin, A., Hornstrup, A., et al.; ApJS 172, 561 (2007).
Erben, T., Schirmer, M., Dietrich, J.P., et al.; Astron. Notes 326, 432, (2005).
Heymans, C., van Waerbeke, L., Bacon, D., et al.; MNRAS, 368, 1323, (2006).
Schirmer, M., Erben, T., Schneider, P., et al.; A&A 420, 75, (2004).
Vikhlinin, A., McNamara, B. R., Forman, W., et al.; ApJ 502, 558, (1998).
Vikhlinin, A., Burenin, R. A., Ebeling, H., et al.; subm. to ApJ, astro-ph/0805.2207.